© 2016. Published by The Company of Biologists Ltd | Journal of Experimental Biology (2016) 219, 920-932 doi:10.1242/jeb.042317

REVIEW

Flapping wing aerodynamics: from insects to vertebrates

Diana D. Chin* and David Lentink

ABSTRACT

More than a million insects and approximately 11,000 vertebrates utilize flapping wings to fly. However, flapping flight has only been studied in a few of these species, so many challenges remain in understanding this form of locomotion. Five key aerodynamic mechanisms have been identified for insect flight. Among these is the leading edge vortex, which is a convergent solution to avoid stall for insects, bats and birds. The roles of the other mechanisms – added mass, clap and fling, rotational circulation and wing–wake interactions – have not yet been thoroughly studied in the context of vertebrate flight. Further challenges to understanding bat and bird flight are posed by the complex, dynamic wing morphologies of these species and the more turbulent airflow generated by their wings compared with that observed during insect flight. Nevertheless, three dimensionless numbers that combine key flow, morphological and kinematic parameters – the Reynolds number, Rossby number and advance ratio – govern flapping wing aerodynamics for both insects and vertebrates. These numbers can thus be used to organize an integrative framework for studying and comparing animal flapping flight. Here, we provide a roadmap for developing such a framework, highlighting the aerodynamic mechanisms that remain to be quantified and compared across species. Ultimately, incorporating complex flight maneuvers, environmental effects and developmental stages into this framework will also be essential to advancing our understanding of the biomechanics, movement ecology and evolution of animal flight.

KEY WORDS: Aerodynamic mechanisms, Bat, Bird, Flapping flight, Kinematics, Wing morphology

Introduction

Flapping wings are a convergent solution for the powered flight of more than a million insect species (Dudley, 2002), as well as over 1000 species of bat (Shi and Rabosky, 2015) and ∼10,000 bird species (Jetz et al., 2012) living in complex aerial habitats. Many species migrate annually between habitats worldwide, some literally across the globe (Gill et al., 2009); thus, identifying the aerodynamic principles that enable the evolutionary enigma of flight is key to understanding the development, physiology and movement ecology of many insects and vertebrates. Remarkably, these animals evolved to make use of aerodynamic principles different from those used in aircraft to propel themselves through air. Despite recent progress (e.g. Shyy et al., 2013; Cheney et al., 2014; Crandell and Tobalske, 2015; Dial et al., 2008; Elimelech and Ellington, 2013; Kruyt et al., 2015; Lentink et al., 2015; Nabawy and Crowther, 2014; Song et al., 2014), there are still myriad open questions about how animals fly with flapping wings, a form of movement that is less well understood than terrestrial and aquatic forms of locomotion. Our understanding of insect aerodynamics is more advanced than that of vertebrate flight, and this contrast allows us to identify gaps in our knowledge of how vertebrates harness aerodynamic mechanisms to hover and fly forward. We thus begin this review by identifying the key mechanisms that enable insect flight. The leading edge vortex (LEV; see Glossary), a mechanism common to both insects and vertebrates, can be used to bridge the discussion to birds and bats. We proceed by identifying three non-dimensional numbers that dictate how aerodynamic forces are generated in animal flight, and then compare and contrast the forces generated within insect and vertebrate wingbeats. The observed differences are explained through a discussion of the dynamic wing morphologies that are unique to vertebrate flight. Finally, we propose a framework for integrating the aerodynamic mechanisms employed by insects, bats and birds, highlighting current open challenges in the study of flapping flight. Addressing these challenges will be essential to advancing our understanding of the comparative and integrative biomechanics of flight across insects and vertebrates.

Department of Mechanical Engineering, Stanford University, Stanford, CA 94305, USA.

*Author for correspondence (ddchin@stanford.edu)

Insect aerodynamics model

The wing stroke of an insect consists of two translational phases, the downstroke and upstroke, separated by two rotational phases, pronation and supination (see Glossary). By rotating the wing during each stroke reversal, the leading edge of the wing (i.e. the front-most edge of the wing section) always leads (Dickinson et al., 1999). Five key aerodynamic mechanisms have been identified to explain how insects generate aerodynamic force with their wings (Fig. 1). These mechanisms – added mass, absence of stall, rotational circulation, clap and fling and wing–wake interactions – are discussed below and can be combined to form the quasi-steady model of flapping insect flight, which is discussed in the next section.

Added mass

When the wing accelerates and decelerates during startup (Fig. 1A) and stroke reversal (Fig. 1E), it must also start and stop the surrounding air. The air closest to the wing experiences the greatest acceleration and deceleration, and this results in a pressure force that acts on the wing. This effect is experienced as additional wing mass by the structure and muscles that enable the wing to flap. As such, it is generally referred to as the 'added mass' effect, and is often modeled mathematically as a time-variant increase in the inertia of the wing (Lehmann, 2004; Sane, 2003; Sane and Dickinson, 2001). The added inertia increases forces associated with acceleration of the wing, thereby augmenting aerodynamic force generation.

Absence of stall

As the wing translates during the downstroke and upstroke at a high angle of attack (see Glossary), air flow separates around the leading edge, and the separated boundary layer (see Glossary) rolls up into a strong LEV that remains stably attached to the translating wing (Fig. 1B) (Ellington et al., 1996; Lentink and Dickinson, 2009). The flow reattaches to the wing behind this vortex, so that the wing does

Journal of Experimental Biology

Journal of Experimental Biology (2016) 219, 920-932 doi:10.1242/jeb.042317

Glossary

Advance ratio
The ratio of forward flight speed to wingtip speed.

Angle of attack
The angle formed between the wing chord and incident flow velocity.

Boundary layer
The thin viscous flow region adjacent to the surface of the wing.

Coriolis acceleration
The acceleration that results from the movement of mass in a rotating reference frame; this is equal to twice the product of the rotational velocity of the reference frame and the radial velocity of the mass relative to that frame.

Fixed wing aspect ratio
The ratio of the wing length from tip to tip to average chord length, calculated as wing length squared divided by surface area.

Flapping wing aspect ratio
The ratio of wing radius from the shoulder to the wingtip to average chord length, calculated as wing radius squared divided by surface area.

Fluid
A substance, typically a gas or liquid, that deforms (flows) continuously under a shear stress (force per unit area acting parallel to a surface element), such as air or water.

Inviscid
Idealized airflow without viscosity (no friction).

Kramer effect
The generation of additional circulation during wing rotation so that flows over both surfaces of the wing join smoothly at the trailing edge.

Leading edge vortex
A vortex formed on the leading edge of wings moving at high angles of attack.

Pronation
The transition from upstroke to downstroke, when the ventral surface of the wing rotates to face downwards.

Reynolds number
The ratio of inertial to viscous forces.

Rossby number
The ratio of inertial to Coriolis forces.

Supination
The transition from downstroke to upstroke, when the ventral surface of the wing rotates to face upwards.

Turbulence
Flow characterized by random, chaotic motion – this motion can also mix higher energy flow into the boundary layer, which can help delay separation.

Vorticity
The curl (rotation) of the flow velocity.

not stall and is thus able to transfer a greater downward momentum to the fluid (see Glossary) than would be possible under fixed-wing steady-state conditions (Dickinson et al., 1999; Ellington et al., 1996). Stall avoidance through LEV stabilization is the primary mechanism for augmenting lift during mid-downstroke and mid-upstroke. However, because the resultant pressure force acts normal to the wing surface, drag is also significantly increased by the presence of an LEV (Sane, 2003). For fixed wings translating at high angles of attack, the LEV continues to grow until the flow can no longer reattach; consequently, the flow separates from the wing. Thus, this effect is often referred to in the literature as ‘stall delay’ or ‘delayed stall’. However, this name may be misleading for flapping flight; remarkably, the LEV remains stably attached to a flapping wing after it is formed at the start of the stroke. Therefore, stall is avoided rather than delayed. During midstroke, the LEV is stabilized by centripetal and Coriolis accelerations (see Glossary) that drive and guide axial flow along the span of the wing. These accelerations are induced by the revolving motion of the wing around its base (Ellington et al., 1996; Lentink and Dickinson, 2009; Kruyt et al., 2015). The LEV has been observed in experiments and simulations for a diverse range of insects, including fruit flies (Lehmann and Dickinson, 1998; Sun and Tang, 2002), hawkmoths (Willmott et al., 1997; Liu et al., 1998), dragonflies (Wang and Sun, 2005) and bumblebees (Bomphrey et al., 2009).

Rotational circulation

During pronation and supination, the rotation of the wing generates circulation in the surrounding air (Fig. 1C) that is proportional to the angular velocity of wing rotation (Sane, 2003). This rotational effect, the Kramer effect (see Glossary), decreases in magnitude as the axis of rotation moves towards the trailing edge of the wing. Based on the duration and timing of the rotation relative to each wing stroke, this effect can either enhance or attenuate forces generated during translation (Sane, 2003; Sane and Dickinson, 2001). In advanced rotation, the wing flips before stroke reversal, which increases lift. By contrast, in delayed rotation, the wing flips after stroke reversal, so the leading edge rotates forwards relative to the translational direction and generates a downwards force (negative lift). Symmetric rotation, when the wing flips during stroke reversal, leads to a positive peak in lift forces before stroke reversal and a negative peak after stroke reversal (Dickinson et al., 1999; Lehmann, 2004). Although many studies focus primarily on lift, to assess the impact of the Kramer effect from a performance perspective, we must also consider drag and power requirements. Drag increases monotonically with flip duration (Sane and Dickinson, 2001), and symmetric rotations require the least power per unit lift (Sun and Tang, 2002); therefore, rapid, symmetric rotations are best for efficient flight. However, other combinations of rotation timing and duration are more useful for maneuvering. In hovering flight, rotational effects have been found to contribute up to 35% of lift in robotic model fruit flies and up to 50% in robotic hoverflies (Dickinson et al., 1999). Note, however, that these values may not be quantitatively accurate for real fruit flies and hoverflies, because the kinematics of the robotic models differ from those of the real insects; such kinematic differences can lead to significant discrepancies in measured aerodynamic forces (Bos et al., 2008). Nevertheless, these lift contribution values should provide a reasonable estimate of the relative importance of the Kramer effect. These results are also assumed to be applicable for forward flight at low or intermediate speeds, when the mean wing tip velocity far exceeds the forward velocity (Sane and Dickinson, 2001; Dickson et al., 2008).

Clap and fling

Further lift enhancement during pronation can result from interaction between the wings (Fig. 1D). After the upstroke, the leading edges of the wings may meet during the ‘clap’. This causes the opposing air circulations on each wing to cancel one another out, reducing the vorticity (see Glossary) shed from the trailing edge during the next stroke. Consequently, the wings can generate circulation at a faster rate and extend the period of lift generation during the following downstroke (Lehmann, 2004). In addition, the fluid pushed out from between the wings during this motion can help to enhance thrust. Of course, the ‘clap’ may also simply be a result of efforts to maximize the stroke amplitude, which can greatly increase flight forces (Sane, 2003). As the wings continue to pronate, the leading edges separate first during the ‘fling’ or ‘peel’.

Journal of Experimental Biology (2016) 219, 920-932 doi:10.1242/jeb.042317

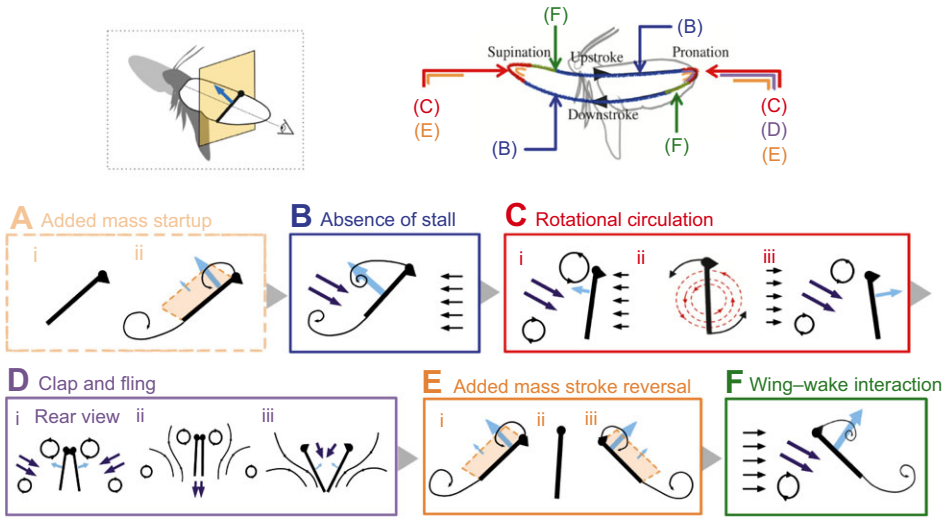

Fig. 1. Complex aerodynamic mechanisms underpin insect flight. (A) As the wing begins to accelerate, the fluid near it must accelerate too, which the wing experiences as 'added mass' (shaded orange region). This fluid acceleration increases the pressure force acting on the wing. (B) During mid-upstroke and mid-downstroke, a leading edge vortex forms, which prevents stall. This process is often referred to as 'stall delay' and greatly enhances lift. (C) During supination and pronation, additional vortex circulation (red arrows) is generated. The magnitude and direction of the resulting force enhancement depends on how the wing rotation is timed with respect to translation: advanced, symmetric or delayed. The wing is shown (i) immediately before, (ii) during and (iii) immediately after rotation. (D) (i) As the wings come together during the 'clap', opposing circulations cancel out. (ii) Fluid pushed out from between the wings aids thrust, and trailing edge vorticity is shed as stopping vortices. (iii) When the wings part during the 'fling', new fluid rushes in, which speeds up circulation generation as translation begins. (E) Added mass effects come into play again as the wing (i) decelerates for (ii) rotation and (iii) accelerates for translation. (F) Interactions of the wing with the wake generated during the previous stroke may lead to a peak in aerodynamic forces immediately following stroke reversal. Mechanisms shown in panels with solid borders (B–F) are then repeated as wingbeats continue. The relative timings of the mechanisms during each wingbeat are indicated in the upper right diagram. In all panels, the wing is represented by its chord, drawn from a point of view directed along the span-wise axis of the wing, as shown in the upper left diagram. Airflow direction is indicated by black arrows, induced velocity is indicated by dark blue arrows and net forces are represented by light blue arrows. Black triangles indicate the top surface of the leading edge. Figures adapted from Sane (2003), with permission.

The region of lower pressure between the wings sucks in fluid, which also helps to generate bound circulation more rapidly as the wings begin the downstroke (Sane, 2003; Lehmann, 2004). The combined interaction of the wings during pronation is often referred to as the 'clap and fling', 'clap and peel' or the Weis-Fogh effect. This mechanism can enhance lift by up to 15%, but this value varies widely across experiments (Lehmann, 2004). Clap and fling is not used continuously, but rather for more demanding flight behaviors such as when carrying loads, making sharp turns or during take-off and climbing flight (Lehmann, 2004; Wakeling and Ellington, 1997; Sunada, 1993). Although many insect species, including butterflies, chalcid wasps, fruit flies, Diptera and damselflies, show variations of this mechanism (Lehmann, 2004; Weis-Fogh, 1973), some species do not utilize it at all, suggesting that clap and fling is a specialization (Wakeling and Ellington, 1997; Dickinson et al., 1999). It is also hypothesized that this mechanism is used by vertebrates during more strenuous flight behaviors (Weis-Fogh, 1973); in fact, clap and fling has been observed during the slow flight of diamond doves (Crandell and Tobalske, 2015).

Wing–wake interaction

During stroke reversal, the wing can 'capture' vortices shed during the previous stroke (Fig. 1F), which occur in a region known as the wake. In doing so, some of the energy lost from the previous stroke is supposedly recovered from the air, thereby improving the overall efficiency of force production. This unsteady aerodynamic effect is known as wake capture or wing–wake interaction. It is thought to result in a peak in aerodynamic forces immediately following stroke reversal, the magnitude and direction of which depends on the phase relationship between rotation and translation (Dickinson et al., 1999). The wing–wake interaction may contribute up to 25% of total lift when combined with clap and fling during hovering, and its relative importance is assumed to increase with stroke amplitude (Sane and Dickinson, 2001). This effect has been qualitatively observed in butterflies (Srygley and Thomas, 2003), and it has been quantified as the difference between the measured and predicted forces in a robotic fruit fly (Dickinson et al., 1999). Flow measurements suggest a correlation between vortices near the wing and this difference. We cannot, however, assume that this difference is a direct result of wing interactions with wake vortices, because there is no aerodynamic model to predict the magnitude and phase of forces resulting from wing–wake interactions. These forces are also difficult to quantify because the wing–wake interactions inevitably alter fluid velocities and coherent structures in the wake. Many vortex wake studies rely on particle image velocimetry (PIV) to obtain measurements of these velocity fields, and are thus unable to isolate the aerodynamic effect that the wake interactions have on the flying animal (Bomphrey, 2012).

Quasi-steady model

Quasi-steady models allow for an estimate of aerodynamic forces to be calculated. The quasi-steady assumption is that fluid dynamic forces do not depend on their time history; instead, they only depend on instantaneous wing kinematics such as velocities and accelerations. A quasi-steady model for insect flight is of particular interest because it simplifies the first four of the aerodynamic mechanisms discussed above (added mass, absence of stall, rotational circulation and clap and fling) into manageable equations (Box 1). Note that wake capture forces are excluded from this model, because they are poorly understood and inherently dependent on flow history. A quasi-steady model incorporating both translational and rotational effects can capture the time course of

Journal of Experimental Biology (2016) 219, 920-932 doi:10.1242/jeb.042317

Box 1. Quasi-steady methods for estimating aerodynamic forces of flapping animal wings

A Quasi-steady wing (or blade) element theory

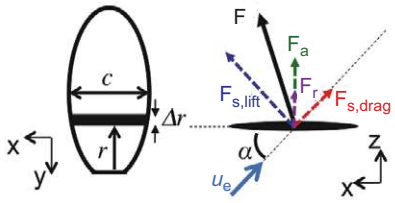

$$F=F_{s,lift}+F_{s,drag}+F_r+F_a+F_{Wake\ capture}$$

Translational lift

$$F_{s,lift}=\Sigma\tfrac{1}{2}\rho c||u_e||^2C_L(\alpha)\Delta r$$

Translational drag

$$F_{s,drag}=\Sigma\tfrac{1}{2}\rho c||u_e||^2C_D(\alpha)\Delta r$$

Rotational force

$$F_r=\Sigma C_r\rho\dot{\alpha}c^2||u_e||\Delta r$$

Added mass force

$$F_a=\Sigma\frac{\rho\pi c^2}{4}\left\{\frac{u_e\cdot\dot{u}_e}{||u_e||}\sin\alpha+||\dot{u}_e||\alpha\cos\alpha\right\}\Delta r$$

B Actuator disc theory

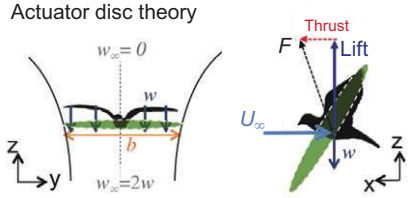

$$F\approx L=-2\rho A_d w^2$$

C Vortex theory

$$F\approx L=\rho\Gamma Ub$$

i

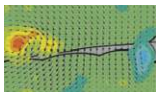

$$\Gamma=\int_A\frac{\partial w}{\partial x}-\frac{\partial u}{\partial z}dA$$

ii

$$\Gamma_{LEV}=\pi d_{LEV}u_\theta$$

iii

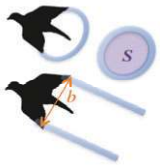

$$\Gamma_{ideal}=\frac{WT}{\rho S}$$

$$\Gamma_{deal}=\frac{W}{\rho Ub}$$

The current quasi-steady insect wing model (Dickson et al., 2008; shown in A) calculates total force on the wing by summing the listed force components along the span for wing elements with chord c and width Δr. $\mathbf{F}_{s,lift}$ acts perpendicular to the wing velocity (u_e), and $\mathbf{F}_{s,drag}$ opposes velocity. $\mathbf{F}_r$ and $\mathbf{F}_a$ act normal to the wing surface, with $\mathbf{F}_a$ pointing opposite to wing acceleration, and $\mathbf{F}_r$ pointing dorsally during supination and ventrally during pronation. No model exists for wake capture. Translational lift (C_L) and drag (C_D) coefficients are measured as functions of the angle of attack (α) with a spinning wing. Harmonic functions have been fitted to this data for fruit flies (Dickinson et al., 1999) and hummingbirds (Kruyt et al., 2014). The rotational force coefficient (C_r) and added mass coefficients have been calculated using inviscid flow theory (Dickson et al., 2008). In the equations presented in A, ρ represents air density, $\dot{\alpha}$ represents angle of attack velocity and $\dot{u}_e$ represents wing acceleration. An alternative method of estimating aerodynamic forces, actuator disc theory (shown in B), estimates lift as the product of mass flux through the stroke plane area, A_d (represented by the green shaded area), and twice the induced velocity, w (Muijres et al., 2011a). In contrast, inviscid vortex theory (shown in C) estimates lift as the product of air density, circulation (Γ), velocity (U) and wingspan (b). Circulation equations are given for: (i) a general velocity field with area A (image shows a velocity field derived from PIV measurements and colored based on relative vorticity, adapted from Muijres et al., 2008, with permission); (ii) an LEV with average diameter d_{LEV} and swirl velocity at the edge of the vortex u_θ; and (iii) vortices shed by straight-flying animals with body weight W. These vortices are modeled either as elliptical vortex loops with projected horizontal area S and period T, for slow flight (upper bird), or as vortex lines called tip vortices separated by wingspan b during fast flight (lower bird; Hedenstrom et al., 2006; Hubel et al., 2010; van den Berg and Ellington, 1997).

aerodynamic force generation with reasonable biological accuracy, but not with mechanistic precision (Sane, 2003; Lehmann, 2004). As with most ad hoc models, these quasi-steady models are grounded in theory, but typically require empirical data to determine the time-invariant parameters. Translational lift and drag coefficients, for example, have been found experimentally by revolving model insect wings at a constant velocity and angle of attack (Dickinson et al., 1999). However, a recent model by Nabawy and Crowther (2014) improves upon the generalizability of existing quasi-steady models by parameterizing wing geometry and kinematics. This enables the application of the model to different insects without detailed kinematic recordings, allowing more comparative studies (Nabawy and Crowther, 2014).

Two other quasi-steady methods for estimating aerodynamic forces rely on measuring flow instead of wing kinematics. These flow measurements generally involve using PIV to capture the wake below or behind the flying animal. The first method models the induced velocity of the flapping wings analogously to that of helicopter blades or an actuator disc (Box 1). By measuring this velocity and estimating the mass flux through the disc, the resulting lift can be estimated based on the rate of change in the downwards momentum. Wake measurements during forward flight can also be used to measure the wake width for a more accurate estimate of the mass flux throughout a wingbeat. The actuator disc theory has the benefit of greater simplicity compared with the kinematics-based quasi-steady model described above. However, the actuator disc theory only estimates vertical lift production and corresponding induced power. Thrust forces are assumed to be negligible, and the model cannot be used to estimate temporal or spatial variations during a wingbeat (Muijres et al., 2011a).

The second method for estimating aerodynamic forces relies on using the vorticity derived from velocity field measurements of the wakes. A rough estimate of the generated lift can then be calculated based on inviscid vortex theory (Box 1) (Hedenstrom et al., 2006; Hubel et al., 2010). When the wake is thin near the trailing edge, the velocity field in a plane perpendicular to the wake can be used to

Journal of Experimental Biology (2016) 219, 920-932 doi:10.1242/jeb.042317

derive a good approximation of aerodynamic forces. However, thrust is often overestimated if the wake is not thin, as is the case for hovering birds (Minotti, 2011). The PIV plane may also be an imperfect representation of the flow because of wake deformations that occur in time and space (Bomphrey, 2012). Additionally, accounting only for vortex forces results in errors due to the omission of fluid acceleration around the wing. Direct numerical simulations have shown that local accelerations due to unsteady inertial effects are non-negligible in flapping flight; thus, time-resolved velocity measurements are needed to capture local vertical accelerations and more accurately determine lift generation (Wang et al., 2013). To resolve the net force accurately, the velocity field needs to be both temporally and spatially resolved.

A convergent solution for avoiding stall: leading edge vortices

Compared with what we know about insect flight, our current understanding of bird and bat aerodynamics is limited owing to the greater morphological complexity of vertebrate wings and the turbulent flow associated with their flight at intermediate Reynolds numbers (see Glossary). Nevertheless, a number of aerodynamic mechanisms have been shown to enhance lift across both insects and vertebrates; in particular, the LEV has been identified as a convergent solution for preventing stall. At high angles of attack, LEVs have been observed across a wide range of biological wings (Fig. 2) that range in complexity from stiff-winged plant seeds (Lentink et al., 2009) to bird wings that can change shape (i.e. morphing wings) (Muijres et al., 2012; Videler et al., 2004). Based on studies of robotic insects, this aerodynamic mechanism may enhance lift by up to 45% in hovering fruit flies (Dickinson et al., 1999) and support up to two-thirds of the lift during the downstroke of hovering hawkmoths (van den Berg and Ellington, 1997). Among vertebrates, the LEV can increase lift by up to 40% in slow-flying bats (Muijres et al., 2008), and it represents up to 26% of the total lift in hovering hummingbirds (Warrick et al., 2009) and up to ∼50% of the lift in some forward-flying birds (Muijres et al., 2012). However, these estimates of vertebrate lift enhancement may only be rough approximations of the true values, because they are based on the quasi-steady method that uses inviscid vortex theory (Box 1). As described previously, this method does not account for unsteady effects, which may become particularly significant during stroke reversal when the LEV is shed and regenerated.

Comparing insect versus vertebrate aerodynamics: informative dimensionless numbers

The convergent use of the LEV among insects and vertebrates suggests that these animals may employ other common aerodynamic mechanisms. Comparing aerodynamics across insects and vertebrates may therefore extend our limited understanding of bat and bird flight. Given the wide array of different variables related to the wing morphology and flapping kinematics of insects and vertebrates, how can their flapping wing aerodynamics best be compared? Non-dimensional parameters combining the most relevant variables that describe the properties of air, wing morphology and kinematics provide a useful means for comparing such diverse groups of animals. In particular, parameters that govern aerodynamic mechanisms – such as the formation of stable LEVs – may offer the greatest comparative insight. Here, we identify and discuss three particularly informative dimensionless numbers: the Reynolds number (*Re*), the Rossby number (*Ro*) and the advance ratio (*J*) (see Glossary). These numbers are not empirical, but are key non-dimensional parameters of Newton's law for fluids (represented by the Navier–Stokes equations), expressed for flapping wings (Lentink and Dickinson, 2009). These three parameters are shown in Fig. 3, and provide the context for comparing insect and vertebrate aerodynamics.

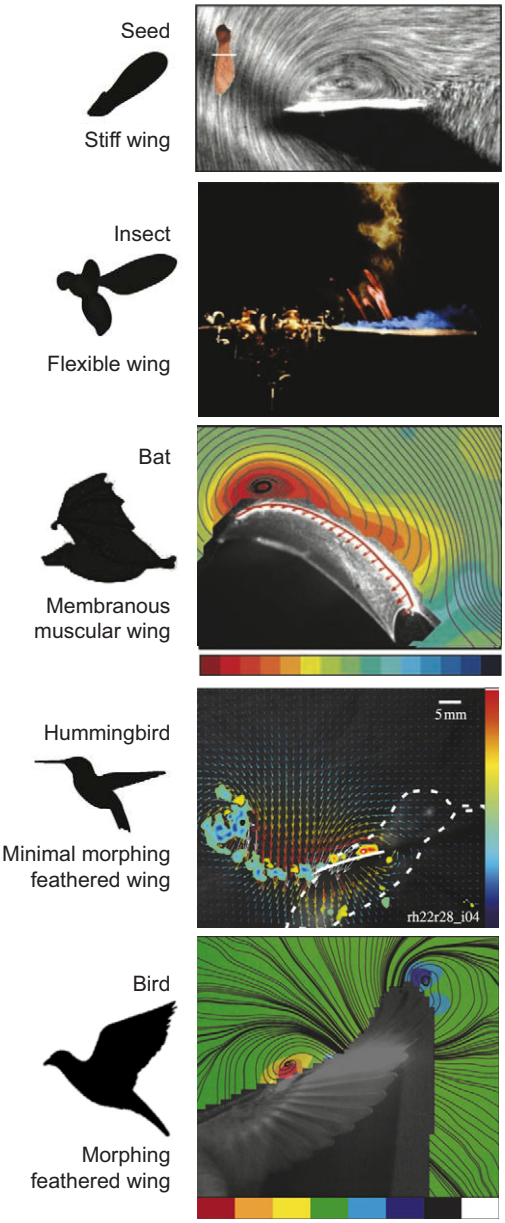

Fig. 2. The leading edge vortex (LEV) is a convergent solution for high lift across body plans. Stable LEVs have been found in (top to bottom): an auto-rotating maple seed (Lentink et al., 2009), a model hawkmoth (*Manduca*) flapper (Ellington et al., 1996), Pallas' long-tongued bat, *Glossophaga soricina* (Muijres et al., 2008), the rufous hummingbird, *Selasphorus rufus* (Warrick et al., 2009), and a pied flycatcher, *Ficedula hypoleuca* (Muijres et al., 2012). The LEV images shown for the seed and insect wing are from smoke visualizations, and those for the vertebrate wings are from particle image velocimetry (PIV) measurements. The local bat wing profile and relative motion are shown by the red curve and arrows. The hummingbird wing profile is shown by the white curve, with the dashed body outline superimposed for reference. Color bars in PIV images refer to vorticity ranges, scaled from −1750 (red) to 1750 s^{-1} (black) for the bat, −6000 (blue) to 6000 s^{-1} (red) for the hummingbird, and −2000 (red) to 2000 s^{-1} (white) for the bird. All images are reproduced with permission.

Journal of Experimental Biology (2016) 219, 920-932 doi:10.1242/jeb.042317

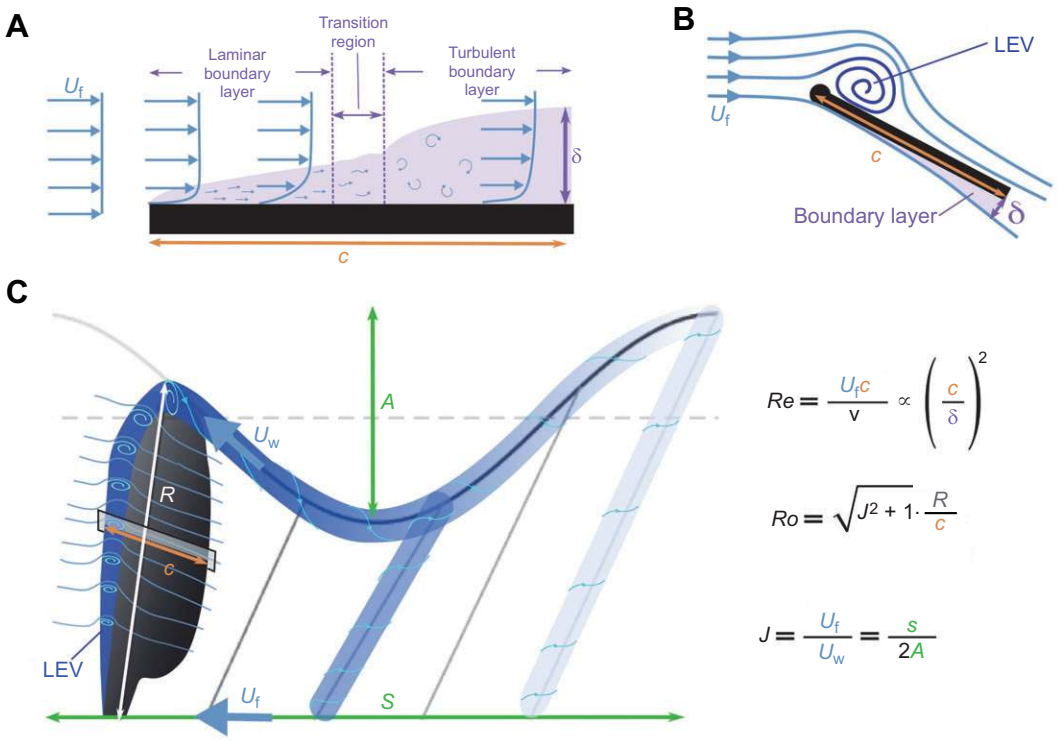

Fig. 3. Non-dimensional parameters that determine flapping wing aerodynamics. Three non-dimensional numbers that relate air, kinematic and morphology parameters to key flow phenomena in flapping animal flight – the Reynolds number (*Re*), advance ratio (*J*) and Rossby number (*Ro*) – can be interpreted visually as length scale ratios (Lentink and Dickinson, 2009). (A) Transition of the wing boundary layer from laminar to turbulent flow depends on *Re*, which is proportional to the square of the chord length, *c*, measured in boundary layer thickness, δ: $Re \propto (c/\delta)^2$. At the high *Re* of vertebrates, the chord length is much larger than the boundary layer thickness – compare this with insects, which have relatively thick viscous boundary layers. U_f, forward velocity. Figure adapted from Shyy et al. (2013), with permission. (B) The stability of the leading edge vortex on a wing swinging around a 'shoulder' joint depends on *Ro*, which is equal to the wing radius, *R*, divided by chord length, *c*, during hovering flight when *J*=0 (the boundary layer on the lower side corresponds to A). Figure adapted from Sane (2003), with permission. (C) The interactions of a vortex wake with the flapping wing depend on *J*, which is equal to the forward distance traveled by the wing base, *s*, divided by the total distance traveled by the wingtip in the stroke plane, 2*A*, during one wingbeat. The wing is shown during mid-stroke, when a stable LEV is present (the cross-section corresponds to B). The LEV connects to the tip vortex and is shed after each half-stroke. *J* governs the resulting wake dynamics and the interactions of the wake with the wing. U_w, wingtip velocity in the stroke plane; ν, kinematic viscosity of the fluid. During forward flight, *Ro* increases with *J*, which explains why less-prominent LEVs are formed at high *J* in animal flight. Figure adapted from Lentink and Dickinson (2009), with permission.

The parameter that differs the most between insect and vertebrate flight is *Re*, the ratio between inertial and viscous forces in the airflow. *Re* can range up to six orders of magnitude among flying animals, from values close to 1 for the smallest hovering insects to ∼1,000,000 for a diving falcon (Swartz et al., 2008). Beyond *Re* of ∼10,000, the regime in which most vertebrates fly, the boundary layer flow can become transitional or turbulent, which governs aerodynamic performance optimization in a way that is not yet fully understood for bats and birds (Elimelech and Ellington, 2013; Lentink and de Kat, 2014; van Bokhorst, et al., 2015). Studies have shown that *Re* has important implications for the structure of the LEVs formed on insect and vertebrate wings (Fig. 4A). For example, at the lower *Re* values associated with insect flight, axial flow in the LEV increases with *Re* (Birch et al., 2004). As *Re* continues to increase to values associated with vertebrate flight, the LEV may bifurcate or burst (Lentink and Dickinson, 2009). Although *Re* is well suited for describing the average flow around fixed wings, it is not sufficient to describe the flow around flapping wings, which accelerates and decelerates significantly during each wingstroke. We thus require two more dimensionless numbers, namely *Ro* and *J*, to characterize the locally accelerating flow around flapping wings. Unlike *Re*, these two numbers are remarkably similar across all animals with flapping wings.

When flapping wings 'translate' during the downstroke and upstroke, they are actually revolving about the shoulder joint (or equivalent point of rotation). *Ro* is used to characterize these rotational effects by describing the ratio of inertial to Coriolis forces. For hovering flight, *Ro* can also be interpreted more intuitively as the aspect ratio (see Glossary) of a single wing with respect to the center of rotation (the shoulder joint). It ranges roughly from 1 to 10, with average values between 3 and 4 for hovering insects and vertebrates (Fig. 4B) (Lentink and Dickinson, 2009). Flapping wings can be approximated experimentally by spinning wings during midstroke, when angular velocity is near constant. When this is the case, *Ro* governs the ability of the wing to maintain a stable LEV, because it is inversely proportional to the centripetal and Coriolis accelerations that induce the stabilizing span-wise flow on spinning and flapping wings. LEV stabilization requires *Ro* of ∼4 or lower (Lentink and Dickinson, 2009; Kruyt et al., 2015).

The advance ratio, *J*, is used to characterize the effects resulting from the reciprocating motion of a flapping wing. *J* is the ratio of the forward flight velocity component of the wing tip (U_f) to the velocity component in the stroke plane of the flapping wing (U_w). The wingtip velocity component in the stroke plane can also be expressed as the distance traveled by the wingtip in the stroke plane – twice the peak-to-peak amplitude (*A*), times the flapping frequency (*f*) – so $J = U_f/2Af$. Using this definition, *J* is purely a

Journal of Experimental Biology (2016) 219, 920-932 doi:10.1242/jeb.042317

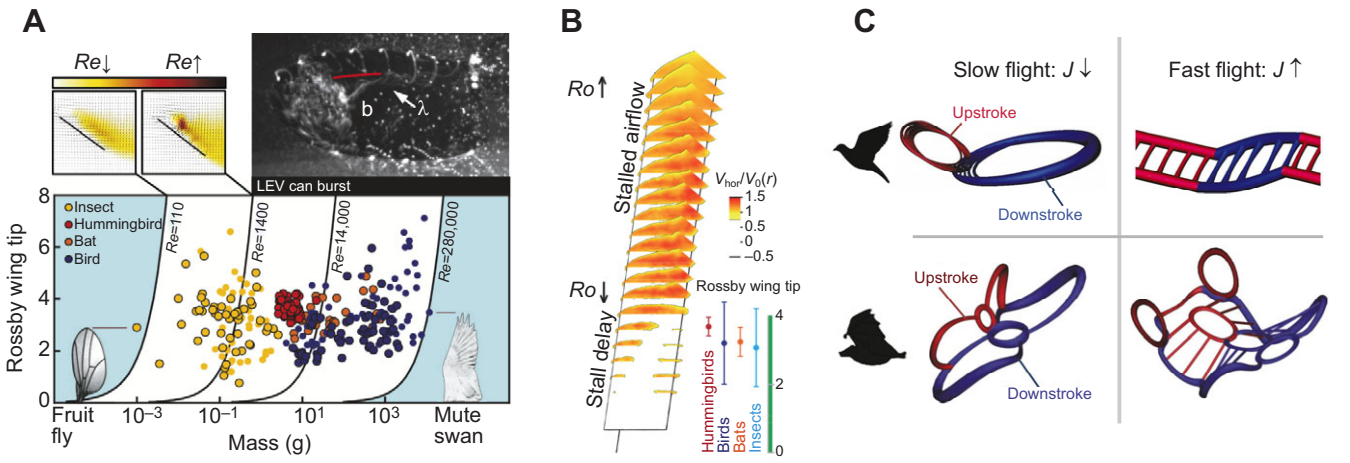

Fig. 4. How leading edge vortex (LEV) and vortex wake formation depends on dimensionless numbers. (A) Reynolds number (*Re*) effect on LEV formation. *Re* ranges over orders of magnitude in animal flight, from 10^2 for small insects to 10^6 for diving falcons. Throughout this range, *Re* significantly influences LEV formation. At the *Re* of insect flight, axial flow in the LEV increases with *Re*. Upper left plots show sectional velocity fields over a wing at *Re*=120 and 1400, superimposed over a color plot of axial velocity; the color bar ranges from 0 (white) to 0.5 m s^{-1} (black). At *Re* over 1400, LEVs may bifurcate (λ) or burst (b) (as shown in the upper right image; bifurcated vortices are separated by the red line), especially when the boundary layer begins to transition from laminar to turbulent flow. This transition occurs at $Re \approx 10^4$, which is intermediate to insects and most birds, but where hummingbirds fly. Figures adapted from Birch et al. (2004) and Lentink and Dickinson (2009), with permission. (B) Rossby number (*Ro*) effect on LEV stability. Horizontal air speed distributions (V_{hor}) over a wing revolving at a high angle of attack (45 deg) are shown relative to the wing speed [($V_o(r)$)]. Most flying animal wings fall within *Ro* of 3 to 4, where stall delay is maintained [white regions on the wing, where $V_{hor}/V_o(r)<1$]. As *Ro* increases, the wing becomes unable to maintain a stable LEV, resulting in stalled airflow. During stall, the horizontal air velocity is close to the wing speed, so it sticks to the surface and stands still [colored regions, where $V_{hor}/V_o(r) \approx 1$]. Figure adapted from Kruyt et al. (2015), with permission. (C) Advance ratio (*J*) effect on vortex wake formation and interaction. The structure of the vortex wake is strongly dependent on *J*, which can range from 0 to 5 in animal flight. During slow flight (small *J*), wingtip vortices shed by birds during the downstroke (blue) and upstroke (red) form two distinct loops. Slow-flying bats shed vorticity at their wing base as well as at the wingtip, leading to separate vortex loops for each wing. At cruising speed (large *J*), smaller vortices are shed throughout the stroke cycle, forming a wake structure that resembles a ladder. Figure adapted from Hedenstrom et al. (2007) and Spedding et al. (2003), with permission.

kinematic parameter. However, if we assume that flapping frequency is equivalent to the vortex shedding frequency, then *J* becomes precisely half the inverse of another well-known non-dimensional parameter, the Strouhal number ($St=Af/U_f$). Although *St* is often used in biological literature, it is undefined for hovering flight ($U_f=0$ results in $St=\infty$), so we use *J* for describing both hovering ($J=0$) and forward flight ($J>0$). With *f* defined as the vortex shedding frequency, *J* governs the time scales of vortex growth and shedding in the wake, so different vortex wake structures are formed at different values of *J* (Taylor et al., 2003; Hedenstrom et al., 2007; Spedding et al., 2003; Fig. 4C). Based on the typical ranges of *St* reported for flapping animal flight (Taylor et al., 2003), *J* varies from 0 to 5, with optimal propulsive efficiency at $1.25<J<2.50$. This range has been correlated with higher efficiency of propulsion in both aquatic and aerial locomotion, because, within this range, *J* is optimally tuned to form vortex wake structures associated with efficient thrust development (Triantafyllou et al., 1993; Taylor et al., 2003; Nudds et al., 2004).

In summary, these three key aerodynamic parameters determine the generation of turbulent flow (*Re*), the stability of the LEV (*Ro*) and the formation of an efficient vortex wake (*J*). *Re* differs greatly between insects and vertebrates, whereas *Ro* and *J* are similar for insect and vertebrate flight. The significance of the differences in *Re* and similarities in *Ro* and *J* may be better appreciated by considering scaling effects in the context of these numbers.

Interpreting the aerodynamic implications of body size with dimensionless numbers

The dimensionless numbers *Ro*, *J* and *Re* can provide a useful lens for examining how the flight of insects and vertebrates is affected by the wide range of body sizes of these species. The effects of different body sizes on the aerodynamics of flying animals are often estimated using isometric scaling arguments and empirical allometric relationships. Many power functions have been developed to express flight variables, such as characteristic speeds and the power required for steady horizontal flight, as functions of wing dimensions or body mass (Shyy et al., 2013; Rayner 1988; Norberg, 1990). However, mechanical and physical constraints often lead to deviations from these scaling relationships, and isometry is generally only a reasonable approximation at lower taxonomic levels (Alerstam et al., 2007; Shyy et al., 2013; Rayner, 1988; Norberg, 1990). Thus, to understand the implications of size differences across insects and vertebrates, we instead examine the effects of size on the dimensionless numbers (*Ro*, *J* and *Re*) that govern flapping flight aerodynamics.

The effect of animal size on *Ro* and *J* may not be immediately apparent, because these values are fairly consistent across the diverse groups of flying animals. *J*, for example, is a function of flapping amplitude, flight speed and wingbeat frequency, all of which scale with mass. *Ro* is a function of *J* and the single-wing aspect ratio, which also scales with mass, and yet most animals fly within a narrow range of *Ro* and *J*, regardless of their size. This consistency can be explained by the constraints associated with sustaining flight performance; to maintain a stable LEV, *Ro* must be ~4 or less, and for optimal forward flight, *J* must be between 1.25 and 2.5. In light of the fact that animals with comparable behavior or niches tend to exhibit similar flight morphology (Rayner, 1988; Norberg, 1990), we may also interpret the consistency of these parameters as less of a constraint, and more of a strategy to optimize flight performance for necessary behaviors. In either case, we see that the insensitivity of *Ro* and *J* to differences in scale make these

numbers useful for understanding aerodynamic performance across a wide range of animal sizes.

In contrast, size has a much greater effect on *Re* and the aerodynamics that it governs. Small and lightweight insects tend to have shorter wings and fly at lower speeds, and thus at lower *Re*. For very low values of *Re* (between 1 and 1000), fluid interaction between the wings and surroundings is limited; viscous forces damp out external disturbances in the flow and limit the spatial and temporal extent of wakes (Swartz et al., 2008). In contrast, large birds and bats tend to have longer wings and fly at higher *Re*. In this regime, the boundary layer flow over the wing is more sensitive to turbulence in the atmosphere and other environmental effects. Large animals also tend to generate more turbulence and leave behind longer wakes that dissipate more slowly (Swartz et al., 2008). Because *Re* strongly affects how flow develops close to the wing, vertebrates require different wing morphology and kinematics than insects to generate aerodynamic force.

Wing stroke and morphology functions unique to vertebrates

How do morphological and kinematic features of the flapping wings of flying vertebrates contrast with those of insects and mediate differences in aerodynamic performance? Although there are limited data that can be compared directly, we can compare current lift and drag force estimates resolved within a wing beat for insects and vertebrates (Fig. 5). Most of the force data available for insects and hummingbirds only pertain to hovering flight; thus, to make this comparison, we pooled data for hovering insects and hummingbirds with that derived from slow-flying (~2–3 m s^{-1}) bats and birds. Although insects in forward flight generate more lift during the downstroke than the upstroke (Willmott et al., 1997; Ennos, 1989; Young et al., 2009; Henningsson and Bomphrey, 2013), many hovering insects support their body weight relatively symmetrically during the upstroke and downstroke (Dickinson et al., 1999). In contrast, most bats and birds support their body weight primarily during the downstroke across all flight speeds.

Insect wings exhibit significant flexibility that can reduce drag or increase lift (Zhao et al., 2010; Du and Sun, 2010; Young et al., 2009), but the only active control that insects have over these wing deformations comes from forces applied at the wing base (Wootton, 1981). Flying vertebrates, in contrast, have intrinsic wing musculature that allows for greater control over shape changes during different flight modes. For example, fast-flying birds and those with rounded low-aspect-ratio wings tend to fully flex their entire wing during the upstroke, without generating lift. Another type of upstroke often referred to as the ‘wingtip reversal upstroke’ is used predominately by slow-flying birds, especially those with pointed higher-aspect-ratio wings. This upstroke involves supination of the hand wing, the distal section of the avian wing, using multiple points of rotation within the wing (Crandell and Tobalske, 2011; Hedenstrom et al., 2009; Ros et al., 2011). As the hand wing supinates, the primary feathers separate like a Venetian blind and function as individual airfoils, allowing air to flow through the wing (Hedenstrom et al., 2009; Crandell and Tobalske, 2011). A variety of studies, including those involving wing spinners (Crandell and Tobalske, 2011) and kinematics (Ros et al., 2011; Hedrick et al., 2004), as well as a few flow studies (Warrick et al., 2009; Crandell and Tobalske, 2015), suggest that this upstroke generates some thrust and weight support. The first direct force measurements in animal flight (Lentink et al., 2015) suggest that slow-flying birds that reverse their wingtips during the upstroke support their body weight primarily during the downstroke. Bat wings, which similarly flex during the upstroke and extend during the downstroke, also generate the majority of aerodynamic force during the downstroke (Hedenstrom et al., 2007; Tian et al., 2006). Flow studies at intermediate speeds suggest that bats may also generate a small amount of negative lift and positive thrust at the end of their upstroke with reversed vortex dipoles (Hedenstrom et al., 2009; Muijres et al., 2011b). At higher speeds, these vortex structures become more prominent for two nectar-feeding bats (Muijres et al., 2011b), but fade or disappear altogether for an insectivorous bat (Hubel et al., 2012).

Given that vertebrates seem to generate aerodynamic force primarily during the downstroke across all flight speeds, how does their specialized wing morphology help to facilitate this? Similar to insect wings, bird and bat wings have a sharp leading edge that promotes the formation of a LEV (Videler et al., 2004; Norberg, 1972). Vertebrates can use their arm and hand muscles to actively twist and bend the wing surface within a stroke. For birds, this wing twist reduces the angle of attack along the wingspan, which may help to stabilize the LEV and prevent flow separation (Muijres et al., 2012). Birds can also use their alula, a small winglet attached to the bird’s thumb, as a wing slot to prevent flow separation (Lee et al., 2015; Hedenstrom et al., 2009). Bats can actively optimize the shape of their wing through the use of tiny muscles in the membrane (Cheney et al., 2014) in concert with over two dozen independently controlled joints of deformable bones that stretch the wing (Tian et al., 2006). By flexing their first and fifth digits and/or the leading edge flap between their second and third digits, bats increase the camber, and thus the lift coefficient, of their wings (Hedenstrom et al., 2009; Norberg, 1972). These changes in camber may also help maintain the LEV (Muijres et al., 2008). To fully establish these functions of active twist and camber changes, we need better physical models and novel *in vivo* animal manipulations.

Finally, insect wings are corrugated and covered with scales, hairs and other features that protrude into the boundary layer flow. Bird and bat wing surfaces are similarly architecturally sophisticated, and the boundary layer over vertebrate wings is sensitive to these surface protrusions because *Re* values of these species are above 10,000. If the angle of attack is high enough and the protrusion height is similar to the local boundary layer thickness, the flow over the upper surface of the wing will transition to turbulent flow (van Bokhorst et al., 2015). Turbulent boundary layers are more resistant to flow separation, and allow the high drag and hysteresis effects caused by laminar flow separation to be overcome (Shyy et al., 2013). In swifts, the feather rachides act as ‘turbulator’ strips to force the flow to become turbulent, which dramatically reduces flow separation (van Bokhorst et al., 2015). Similarly, in bats, the ridges formed by digits that project over the dorsal surface may reduce flow separation (Norberg, 1972). There is also behavioral evidence that bats monitor flow on their wings with small hairs on the dorsal surface of their membranous wings; when these hairs are removed, bats fly faster and make wider turns (Sterbing-D’Angelo et al., 2011).

We thus begin to see how vertebrates can control the intermediate *Re* flow over their wings using specialized morphological adaptations. By manipulating the shape of their wings, birds and bats may be able to significantly improve lift during the downstroke by maintaining the LEV, and they may also be able to minimize drag and power during the upstroke. Further studies are needed to quantify these aerodynamic functions.

Journal of Experimental Biology (2016) 219, 920-932 doi:10.1242/jeb.042317

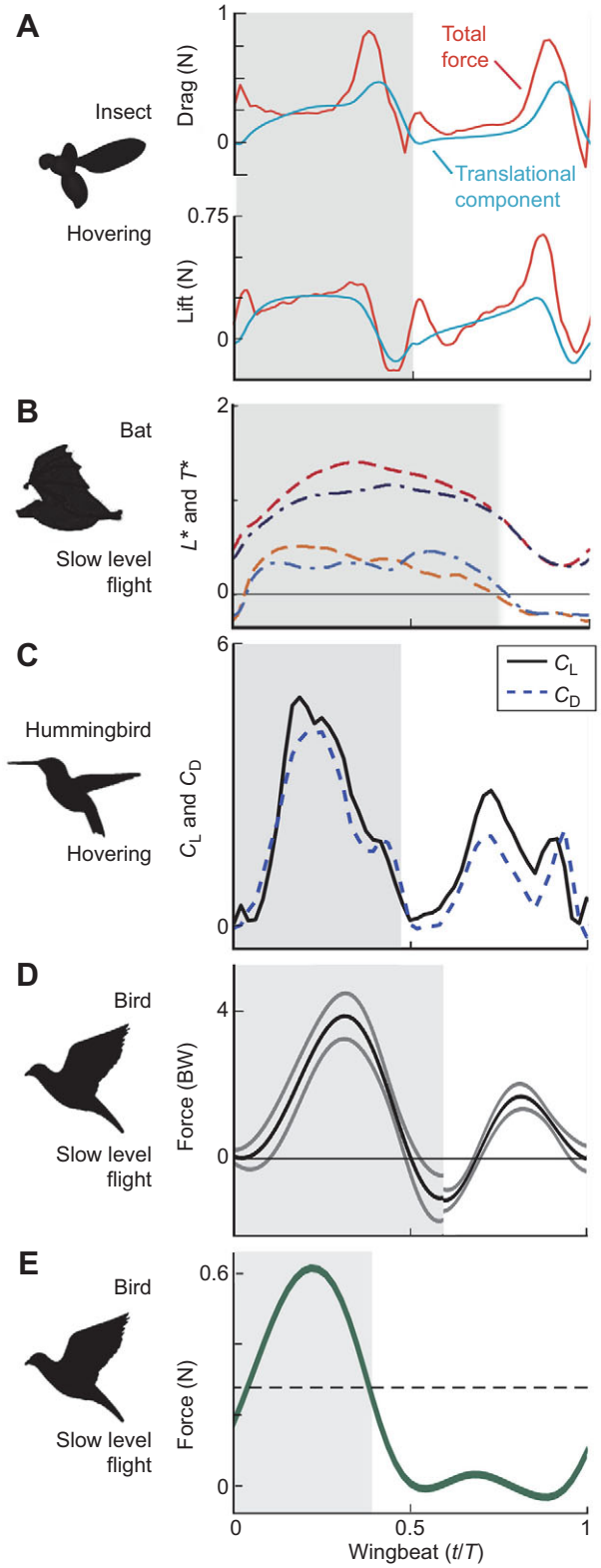

Fig. 5. How flapping wing force within a wingbeat compares among insects, birds and bats. (A) Many hovering insects generate similar lift and drag forces during the downstroke (gray background) and upstroke (white background). Force estimates are based on measurements from a robotic model fruit fly. Figure adapted from Dickinson et al. (1999), with permission. (B) For *Glossophaga soricina* (dashed lines) and *Leptonycteris yerbabuenae* (dash-dotted lines), body-weight-normalized lift (L^*, red and dark blue lines) and thrust (T^*, orange and light blue lines) forces dominate during the downstroke. Results shown are based on vorticity measurements and vortex theory for slow (2 m s^{-1}) forward flight. Figure adapted from Muijres et al. (2011b), with permission. (C) Hovering hummingbirds generate less, but still significant, lift and drag during their upstroke compared with their downstroke. The coefficients of lift (C_L) and drag (C_D) shown are based on computational fluid dynamics. Figure adapted from Song et al. (2014), with permission. (D) Slow-flying pigeons produce much less net aerodynamic force ($|F|$) during the upstroke than the downstroke, based on 3D kinematics and body mass distributions. The force trace shown is the pooled mean±s.d. of the mean $|F|$ for three pigeons, normalized to body weight (BW) and wingbeat duration. The discontinuity is caused by variations in stroke durations. Figure adapted from Ros et al. (2011), with permission. (E) Pacific parrotlets produce little weight support during the upstroke, based on direct force measurements during slow forward flight. Horizontal axis shows time (t) normalized to total wingbeat duration (T). Figure adapted from Lentink et al. (2015), with permission.

An integrative and comparative framework for flapping wings

Using non-dimensional numbers to understand the aerodynamics of flapping animal flight

In spite of morphological and kinematic differences between insect and vertebrate flight, the available aerodynamic mechanisms of force generation, such as the convergent LEV, are governed by the same non-dimensional parameters. Consequently, we infer that animals may employ similar aerodynamic mechanisms if *Ro* and *J* of their flapping wings are similar and *Re* effects are small. Using these parameters, we have organized an integrative and comparative framework of flapping wing aerodynamics as outlined in Fig. 6, which is based on our current knowledge. To determine what research remains to be performed to complete this framework, we have categorized seven aerodynamic mechanisms studied in animal flight by animal group and flight speed in Fig. 7. To streamline the overview, we have grouped diverse 'morphological effects' as the seventh mechanism (light green shading in Fig. 7). The overview reveals that our integrative and comparative understanding of flapping animal flight is remarkably incomplete.

Fig. 7 identifies the many gaps that must be filled to form an inclusive framework for understanding the aerodynamics of flapping animal flight. Aside from the LEV, it is unclear to what degree vertebrates make use of the five key aerodynamic mechanisms that have been identified for insects, particularly wake capture, in addition to morphological effects. In contrast, upstroke effects found in vertebrates have not yet been studied in insects. More quantitative studies will be essential to determine the relative contribution of all of these mechanisms to lift and drag; this is especially true for birds and bats across different flight speeds. However, even among insects, quantitative studies have focused predominately on hovering flight, so more quantitative studies of insect forward flight are also needed. Although several flow studies in recent years have examined forward vertebrate flight, many focus primarily on elucidating vortex wake structures (Bomphrey, 2012; Hubel et al., 2010; von Busse et al., 2014; Henningsson et al., 2014, 2011; Johansson and Hedenstrom, 2009; Hedenstrom et al., 2007, 2006; Muijres et al., 2011b). Also, although some vorticity measurements have been able to account for full weight support, many show deficits in estimated lift, especially at lower speeds when unsteady effects become more significant (von Busse et al., 2014;

Journal of Experimental Biology (2016) 219, 920-932 doi:10.1242/jeb.042317

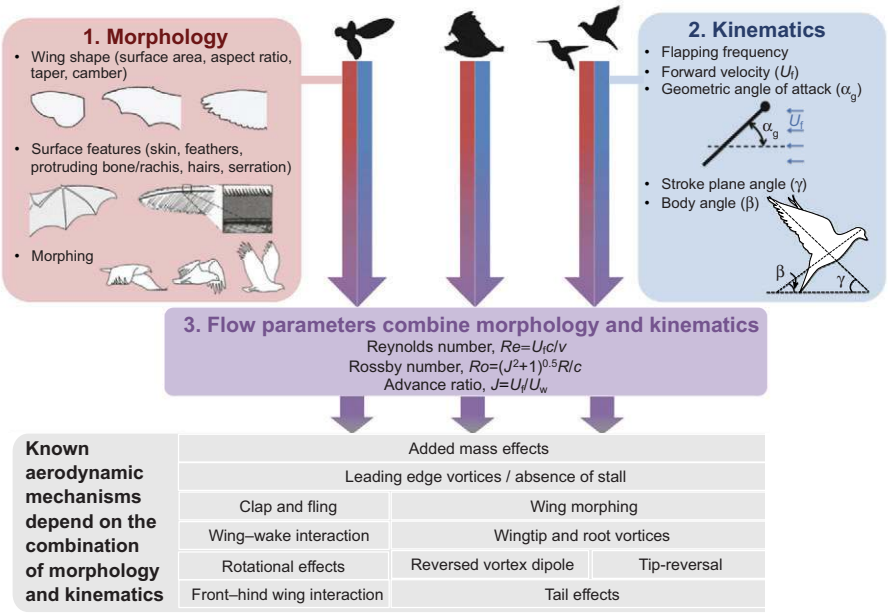

Fig. 6. Integrated framework for modeling flapping flight of insects, bats and birds, based on current knowledge. The aerodynamic mechanisms employed by animals during flapping flight are governed by (1) morphology and (2) flight kinematics. Note that although morphing is also inherently kinematic, it is listed as a morphological factor because the morphing capabilities of insects and vertebrates are strongly dependent on their wing morphology. As shown in Fig. 3, key aerodynamic parameters of morphology and kinematics are combined in three non-dimensional numbers (3): *Re*, *Ro* and *J*. As shown in Fig. 4, these dimensionless numbers are coupled to essential flow phenomena that have been shown to determine aerodynamic performance in animal flight. They can thus be used to efficiently organize the relevance of aerodynamic mechanisms that have been identified in flapping animal flight. Effects that only span the left-most column are those that have been studied primarily for insects. Those that span only the right two columns are those that have been studied primarily for vertebrates. Reversed vortex dipoles and tip reversal have been studied primarily in bats and birds, respectively. Adapted from Hedenstrom et al. (2009), Norberg (2002), Brown (1963) and Shyy et al. (2013), with permission.

Henningsson et al., 2011). Placing an additional emphasis on accurately resolving these forces, especially in the context of different aerodynamic mechanisms, would be a valuable complement to such vortex wake studies.

Furthermore, the quasi-steady model, which uses different equations for modeling lift and drag (Dickinson et al., 1999), is unable to match the time course of either measured force component. Lift predicted by the model typically accounts for only ∼70% of body weight support (Kruyt et al., 2014), so induced drag (drag due to lift) is also underestimated. However, drag tends to be even more greatly underestimated than lift, because total drag force also includes profile drag (drag due to skin friction and the shape of the body), which is difficult to model precisely (Sane and Dickinson, 2001). As a result, quasi-steady model equations vastly underestimate mean drag coefficients, despite the fact that stroke-averaged mean lift coefficients are reasonably accurate for hovering flight (Sane and Dickinson, 2001). Thus, for all animals and modes of flight,

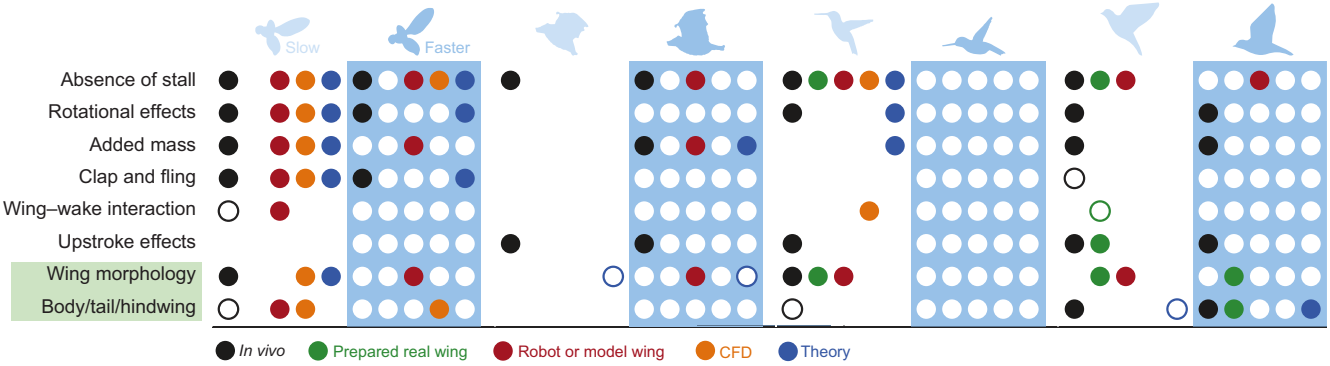

Fig. 7. Gaps in our understanding of aerodynamic mechanisms across insects and vertebrates. Vertically, we list seven aerodynamic mechanisms studied so far for flapping animal flight (the light green shading groups morphological effects as the seventh mechanism). Horizontally, we list animals (insects, bats, hummingbirds and other birds). White columns represent slow flight and light blue columns represent faster flight. Colored circles indicate the methodology used to study the aerodynamic mechanism. CFD, computational fluid dynamics. Filled and open circles indicate quantitative and qualitative studies, respectively. Note that filled circles do not imply direct force measurements, as many studies rely on force estimates based on flow field or kinematic measurements combined with theory. The corresponding references are provided in Tables S1 and S2.

more studies are needed that determine drag. The deficit in drag studies is likely due in large part to the technical challenges inherent in measuring drag compared with lift. Nevertheless, quantifying drag is essential for the determination of the corresponding aerodynamic power requirements, which underpin flight energetics. Finally, more *in vivo* flight studies are necessary to validate results derived from theoretical and physical models. For example, power requirements based on theory and experimental measurements have recently been compared for a fruit bat (von Busse et al., 2014), and similar comparisons would prove valuable for validating models across different species. It would also be of interest to expand research to include other taxa that have not yet been studied owing to technical challenges associated with their relatively large or small size. By filling in these gaps, an overview of the aerodynamic mechanisms used by flying animals can be established. *Re*, *Ro* and *J* can then be used to classify which mechanisms are available for insects, bats and birds based on their wing morphology and motion across specific flight modes.

Understanding flapping flight in its biological context

Many questions remain unanswered in the realm of hovering and forward flight, but even more exist for some of the most interesting animal flight behaviors. Animals that fly with flapping wings have the ability to execute dynamic aerial maneuvers such as obstacle avoidance, sharp turns or the capture of prey in mid-air. The non-dimensional parameters discussed above can adequately cover the essential flow phenomena for straight and level flight. However, to encompass and organize the dynamics and aerodynamic effects relevant to these more complex maneuvers, we suspect that additional parameters are needed.

From a biological perspective, a comprehensive framework will also entail further study of environmental effects on animal flight. For example, studies have shown that hummingbirds change their flight kinematics, such as wingbeat frequency, flapping amplitude and body orientation, to compensate for turbulence (Ortega-Jimenez et al., 2014) and precipitation (Ortega-Jimenez and Dudley, 2012). Bats, in contrast, appear to avoid rain because of both sensory and energy limitations (Voigt et al., 2011). Increased elevation leads to reduced air density and oxygen levels, so altitude is another environmental factor that can affect flight performance. Hummingbirds, for example, can sustain hovering at high elevations at no additional metabolic cost with increased wing size and stroke amplitude. However, at these altitudes, they may not be able to perform complex maneuvers that are more energetically demanding (Altshuler et al., 2004). Given that animals can fly through a range of environmental conditions, quantifying the role of such environmental factors will strengthen our comprehension of the aerodynamic mechanisms that underpin an animal's movement ecology (Swartz, et al., 2008).

Understanding how the aerodynamic mechanisms described above have evolved over time may also lend further insight into the function and importance of these mechanisms. The structures of extinct taxa generally differ too greatly from extant adult animal forms to allow us to fully understand the evolution of animal flight. Instead, researchers often use an evolutionary developmental approach to complement perspectives gained from the fossil record. This approach involves using the morphology and behavior of juvenile animals to gain insight into transitions from ancient ancestors to modern bats and birds (Cooper et al., 2012; Dial et al., 2008; Heers and Dial, 2012). For example, the observation of aerodynamically active wing strokes in the under-developed wings of juvenile birds suggests that distant ancestors of birds may also have benefitted from non-flying wings (Dial et al., 2008). Asymmetric wing motions used by juvenile chukar for aerial righting also suggest another key function of incipient wings – they facilitate controlled aerial maneuvering (Evangelista et al., 2014; Dudley and Yanoviak, 2011). Further studies are needed to determine whether the same aerodynamic mechanisms that are employed by adult birds and bats are also present in the wing strokes of juvenile vertebrates. Elucidating the development of these mechanisms will thus not only aid us in forming a comprehensive model for flapping flight, but may also provide greater insight into the evolution of flight.

Conclusions: challenges and opportunities for understanding flapping animal flight

From our review of the literature, we can identify five key challenges for developing a comprehensive model that provides a mechanistic basis for understanding the physiology, movement ecology and evolution of animal flight. (1) The aerodynamic mechanisms of vertebrates still need to be examined as thoroughly as has been done for insects. (2) Next, the models will need to be extended to work for various flight maneuvers, including climbing, descending and turning flight. (3) Furthermore, these models will need to be validated by *in vivo* measurements of lift and drag forces across flight behaviors, preferably during natural behavior in the field. (4) Quantifying the effects of environmental factors, such as turbulence, precipitation and changes in air density, will advance our understanding of movement ecology. (5) Finally, integrating information on the developmental stage of animal flight will provide a lens for studying the evolution of flight. Overcoming these challenges to gain a deeper understanding of animal flight will be exciting from both a biological and an engineering perspective. It will enable the development of more robust and maneuverable aerial robots, and could also inspire more efficient designs in wind turbines and other technologies that operate in the atmosphere.

Competing interests

The authors declare no competing or financial interests.

Funding

This work was supported by the KACST Center of Excellence for Aeronautics and Astronautics at Stanford.

Supplementary information

Supplementary information available online at
http://jeb.biologists.org/lookup/suppl/doi:10.1242/jeb.042317/-/DC1

References

Alerstam, T., Rosén, M., Bäckman, J., Ericson, P. G. P. and Hellgren, O. (2007). Flight speeds among bird species: Allometric and phylogenetic effects. *PLoS Biol.* **5**, 0050197.

Altshuler, D. L., Dudley, R. and McGuire, J. A. (2004). Resolution of a paradox: hummingbird flight at high elevation does not come without a cost. *Proc. Natl. Acad. Sci. USA* **101**, 17731-17736.

Birch, J. M., Dickson, W. B. and Dickinson, M. H. (2004). Force production and flow structure of the leading edge vortex on flapping wings at high and low Reynolds numbers. *J. Exp. Biol.* **207**, 1063-1072.

Bomphrey, R. J. (2012). Advances in animal flight aerodynamics through flow measurement. *Evol. Biol.* **39**, 1-11.

Bomphrey, R. J., Taylor, G. K. and Thomas, A. L. R. (2009). Smoke visualization of free-flying bumblebees indicates independent leading-edge vortices on each wing pair. *Exp. Fluids.* **46**, 811-821.

Bos, F. M., Lentink, D. Van Oudheusden, B. W. and Bijl, H. (2008). Influence of wing kinematics on aerodynamic performance in hovering insect flight. *J. Fluid. Mech.* **594**, 341-368.

Brown, R. H. J. (1963). The flight of birds. *Biol. Rev.* **38**, 460-489.

Cheney, J. A., Konow, N., Middleton, K. M., Breuer, K. S., Roberts, T. J., Giblin, E. L. and Swartz, S. M. (2014). Membrane muscle function in the compliant wings of bats. *Bioinspir. Biomim.* **9**, 025007. .
Cooper, L. N., Cretekos, C. J. and Sears, K. E. (2012). The evolution and development of mammalian flight. *Wiley Interdiscip. Rev. Dev. Biol.* **1**, 773-779.
Crandell, K. E. and Tobalske, B. W. (2011). Aerodynamics of tip-reversal upstroke in a revolving pigeon wing. *J. Exp. Biol.* **214**, 1867-1873.
Crandell, K. E. and Tobalske, B. W. (2015). Kinematics and aerodynamics of avian upstrokes during slow flight. *J. Exp. Biol.* **218**, 2518-2527.
Dial, K. P., Jackson, B. E. and Segre, P. (2008). A fundamental avian wing-stroke provides a new perspective on the evolution of flight. *Nature* **451**, 985-989.
Dickinson, M. H., Lehmann, F.-O. and Sane, S. P. (1999). Wing rotation and the aerodynamic basis of insect flight. *Science* **284**, 1954-1960.
Dickson, W. B., Straw, A. D. and Dickinson, M. H. (2008). Integrative model of *Drosophila* flight. *AIAA J.* **46**, 2150-2164.
Du, G. and Sun, M. (2010). Effects of wing deformation on aerodynamic forces in hovering hoverflies. *J. Exp. Biol.* **213**, 2273-2283.
Dudley, R. (2002). *The Biomechanics of Insect Flight: Form, Function, Evolution*. Princeton, NJ: Princeton University Press.
Dudley, R. and Yanoviak, S. P. (2011). Animal aloft: the origins of aerial behavior and flight. *Integr. Comp. Biol.* **51**, 926-936.
Elimelech, Y. and Ellington, C. P. (2013). Analysis of the transitional flow field over a fixed hummingbird wing. *J. Exp. Biol.* **216**, 303-318.
Ellington, C. P., van den Berg, C., Willmott, A. P. and Thomas, A. L. R. (1996). Leading-edge vortices in insect flight. *Nature* **384**, 626-630.
Ennos, A. R. (1989). The kinematics and aerodynamics of the free flight of some Diptera. *J. Exp. Biol.* **142**, 49-85.
Evangelista, D., Cam, S., Huynh, T., Krivitskiy, I. and Dudley, R. (2014). Ontogeny of aerial righting and wing flapping in juvenile birds. *Biol. Lett.* **10**, 20140497.
Gill, R. E., Tibbitts, T. L., Douglas, D. C., Handel, C. M., Mulcahy, D. M., Gottschalck, J. C., Warnock, N., McCaffery, B. J., Battley, P. F. and Piersma, T. (2009). Extreme endurance flights by landbirds crossing the Pacific Ocean: ecological corridor rather than barrier? *Proc. R. Soc. B. Biol. Sci.* **276**, 447-457.
Hedenstrom, A., Rosen, M. and Spedding, G. R. (2006). Vortex wakes generated by robins *Erithacus rubecula* during free flight in a wind tunnel. *J. R. Soc. Interface* **3**, 263-276.
Hedenstrom, A., Johansson, L. C., Wolf, M., von Busse, R., Winter, Y. and Spedding, G. R. (2007). Bat flight generates complex aerodynamic tracks. *Science* **316**, 894-897.
Hedenstrom, A., Johansson, L. C. and Spedding, G. R. (2009). Bird or bat: comparing airframe design and flight performance. *Bioinsp. Biomim.* **4**, 015001.
Hedrick, T. L., Usherwood, J. R. and Biewener, A. A. (2004). Wing inertia and whole-body acceleration: an analysis of instantaneous aerodynamic force production in cockatiels (*Nymphicus hollandicus*) flying across a range of speeds. *J. Exp. Biol.* **207**, 1689-1702.
Heers, A. M. and Dial, K. P. (2012). From extant to extinct: locomotor ontogeny and the evolution of avian flight. *Trends Ecol. Evol.* **27**, 296-305.
Henningsson, P. and Bomphrey, R. J. (2013). Span efficiency in hawkmoths. *J. R. Soc. Interface* **10**, 20130099.
Henningsson, P., Muijres, F. T. and Hedenstrom, A. (2011). Time-resolved vortex wake of a common swift flying over a range of flight speeds. *J. R. Soc. Interface* **8**, 807-816.
Henningsson, P., Hedenstrom, A. and Bomphrey, R. J. (2014). Efficiency of lift production in flapping and gliding flight of swifts. *PLoS ONE* **9**, e90170.
Hubel, T. Y., Riskin, D. K., Swartz, S. M. and Breuer, K. S. (2010). Wake structure and wing kinematics: the flight of the lesser dog-faced fruit bat, *Cynopterus brachyotis*. *J. Exp. Biol.* **213**, 34287-33440.
Hubel, T. Y., Hristov, N. I., Swartz, S. M. and Breuer, K. S. (2012). Changes in kinematics and aerodynamics over a range of speeds in *Tadarida brasiliensis*, the Brazilian free-tailed bat. *J. R. Soc. Interface* **9**, 1120-1130.
Jetz, W., Thomas, G. H., Joy, J. B., Hartmann, K. and Mooers, A. O. (2012). The global diversity of birds in space and time. *Nature* **491**, 444-448.
Johansson, L. C. and Hedenstrom, A. (2009). The vortex wake of blackcaps (*Sylvia atricapilla* L.) measured using high-speed digital particle image velocimetry (DPIV). *J. Exp Biol.* **212**, 3365-3376.
Kruyt, J. W., Quicazan-Rubio, E. M., van Heijst, G. F., Altshuler, D. L. and Lentink, D. (2014). Hummingbird wing efficacy depends on aspect ratio and compares with helicopter rotors. *J. R. Soc. Interface* **11**, 20140585.
Kruyt, J. W., van Heijst, G. F., Altshuler, D. L. and Lentink, D. (2015). Power reduction and the radial limit of stall delay in revolving wings of different aspect ratio. *J. R. Soc. Interface* **12**, 20150051.
Lee, S., Kim, J., Park, H., Jabłoński, P. G. and Choi, H. (2015). The function of the alula in avian flight. *Scientific Reports* **5**, 9914.
Lehmann, F.-O. (2004). The mechanisms of lift enhancement in insect flight. *Naturwissenschaften* **91**, 101-122.
Lehmann, F. and Dickinson, M. H. (1998). The control of wing kinematics and flight forces in fruit flies (*Drosophila* spp.). *J. Exp. Biol.* **201**, 385-401.
Lentink, D. and de Kat, R. (2014). Gliding swifts attain laminar flow over rough wings. *PLoS ONE* **9**, e99901.
Lentink, D. and Dickinson, M. H. (2009). Rotational accelerations stabilize leading edge vortices on revolving fly wings. *J. Exp. Biol.* **212**, 2705-2719.
Lentink, D., Dickson, W. B., van Leeuwen, J. L. and Dickinson, M. H. (2009). Leading-edge vortices elevate lift of autorotating plant seeds. *Science* **324**, 1438-1440.
Lentink, D., Haselsteiner, A. F. and Ingersoll, R. (2015). *In vivo* recording of aerodynamic force with an aerodynamic force platform: from drones to birds. *J. R. Soc. Interface* **12**, 20141283.
Liu, H., Ellington, C. P., Kawachi, K., van den Berg, C. and Willmott, A. P. (1998). A computational fluid dynamic study of hawkmoth hovering. *J. Exp. Biol.* **201**, 461-477.
Minotti, F. O. (2011). Determination of the instantaneous forces on flapping wings from a localized fluid velocity field. *Physics Fluids* **23**, 111902.
Muijres, F. T., Johansson, L. C., Barfield, R., Wolf, M., Spedding, G. R. and Hedenstrom, A. (2008). Leading-edge vortex improves lift in slow-flying bats. *Science* **319**, 1250-1253.
Muijres, F. T., Spedding, G. R., Winter, Y. and Hedenstrom, A. (2011a). Actuator disk model and span efficiency of flapping flight in bats based on time-resolved PIV measurements. *Exp. Fluids* **51**, 511-525.
Muijres, F. T., Johansson, L. C., Winter, Y. and Hedenström, A. (2011b). Comparative aerodynamic performance of flapping flight in two bat species using time-resolved wake visualization. *J. R. Soc. Interface* **8**, 1418-1428.
Muijres, F. T., Johansson, L. C. and Hedenstrom, A. (2012). Leading edge vortex in a slow-flying passerine. *Biol. Lett.* **8**.
Nabawy, M. R. A. and Crowther, W. J. (2014). On the quasi-steady aerodynamics of normal hovering flight part II: model implementation and evaluation. *J. R. Soc. Interface* **11**, 20131197.
Norberg, U. M. (1972). Bat wing structures important for aerodynamics and rigidity (Mammalia, Chiroptera). *Z. Morph. Tiere* **73**, 45-61.
Norberg, U. M. (1990). *Vertebrate Flight: Mechanics, Physiology, Morphology, Ecology, and Evolution (Zoophysiology)*. Berlin: Springer.
Norberg, U. M. L. (2002). Structure, form, and function of flight in engineering and the living world. *J. Morph.* **252**, 52-81.
Nudds, R. L., Taylor, G. K. and Thomas, A. L. R. (2004). Tuning of Strouhal number for high propulsive efficiency accurately predicts how wingbeat frequency and stroke amplitude relate and scale with size and flight speed in birds. *Proc. R. Soc. Lond. B.* **271**, 2071-2076.
Ortega-Jimenez, V. M. and Dudley, R. (2012). Flying in the rain: hovering performance of Anna's hummingbirds under varied precipitation. *Proc. R. Soc. B Biol. Sci.* **279**, 3996-4002.
Ortega-Jimenez, V. M., Sapir, N., Wolf, M., Variano, E. A. and Dudley, R. (2014). Into turbulent air: size-dependent effects of von Karman vortex streets on hummingbird flight kinematics and energetics. *Proc. R. Soc. B Biol. Sci.* **281**, 20140180.
Rayner, J. M. V. (1988). Form and function in avian flight. *Curr. Ornithol.* **1**, 1-66.
Ros, I. G., Bassman, L. C., Badger, M. A., Pierson, A. N. and Biewener, A. A. (2011). Pigeons steer like helicopters and generate down- and upstroke lift during low speed turns. *Proc. Natl. Acad. Sci. USA* **108**, 19990-19995.
Sane, S. P. (2003). The aerodynamics of insect flight. *J. Exp. Biol.* **206**, 4191-4208.
Sane, S. P. and Dickinson, M. H. (2001). The control of flight force by a flapping wing: lift and drag production. *J. Exp. Biol.* **204**, 2607-2626.
Shi, J. J. and Rabosky, D. L. (2015). Speciation dynamics during the global radiation of extant bats. *Evolution* **69**, 1528-1545.
Shyy, W., Aono, H., Kang, C. and Liu, H. (2013). *An Introduction to Flapping Wing Aerodynamics*. Cambridge: Cambridge University Press.
Song, J., Luo, H. and Hedrick, T. L. (2014). Three-dimensional flow and lift characteristics of a hovering ruby-throated hummingbird. *J. R. Soc. Interface* **11**, 20140541.
Spedding, G. R., Rosen, M. and Hedenstrom, A. H. (2003). A family of vortex wakes generated by a thrush nightingale in free flight in a wind tunnel over its entire natural range of flight speeds. *J. Exp. Biol.* **206**, 2313-2344.
Srygley, R. B. and Thomas, A. L. R. (2003). Unconventional lift-generating mechanisms in free-flying butterflies. *Nature* **420**, 660-664.
Sterbing-D'Angelo, S., Chadha, M., Chiu, C., Falk, B., Xian, W., Barcelo, J., Zook, J. M. and Moss, C. F. (2011). Bat wing sensors support flight control. *Proc. Natl. Acad. Sci. USA* **108**, 11291-11296.
Sun, M. and Tang, J. (2002). Lift and power requirements of hovering flight in Drosophila virilis. *J. Exp. Biol.* **205**, 2413-2427.
Sunada, S. (1993). Performance of a butterfly in take-off flight. *J. Exp. Biol.* **183**, 249-277.
Swartz, S. M., Breuer, K. S. and Willis, D. J. (2008). Aeromechanics in aeroecology: flight biology in the aerosphere. *Integr. Comp. Biol.* **48**, 85-98.
Taylor, G. K., Nudds, R. L. and Thomas, A. L. R. (2003). Flying and swimming animals cruise at a Strouhal number tuned for high power efficiency. *Nature* **425**, 707-711.
Tian, X., Iriarte-Diaz, J., Middleton, K., Galvao, R., Israeli, E., Roemer, A., Sullivan, A., Song, A., Swartz, S. and Breuer, K. (2006). Direct

measurements of the kinematics and dynamics of bat flight. *Bioinspir. Biomim.* **1**, S10-S18.

Triantafyllou, G. S., Triantafyllou, M. S. and Grosenbaugh, M. A. (1993). Optimal thrust development in oscillating foils with application to fish propulsion. *J. Fluid. Struct.* **7**, 205-224.

van Bokhorst, E., de Kat, R., Elsinga, G. E. and Lentink, D. (2015). Feather roughness reduces flow separation during low Reynolds number glides of swifts. *J. Exp. Biol.* **218**, 3179-3191.

van den Berg, C. and Ellington, C. P. (1997). The three-dimensional leading-edge vortex of a 'hovering' model hawkmoth. *Philos. Trans. R. Soc. Lond. B Biol. Sci.* **352**, 329-340.

Videler, J. J., Stamhuis, E. J. and Povel, G. D. E. (2004). Leading-edge vortex lifts swifts. *Science* **306**, 1960-1962.

Voigt, C. C., Schneeberger, K., Voigt-Heucke, S. L. and Lewanzik, D. (2011). Rain increases the energy cost of bat flight. *Biol. Lett.* **7**, 793-795.

Von Busse, R., Waldman, R. M., Swartz, S. M., Voigt, C. C. and Breuer, K. S. (2014). The aerodynamic cost of flight in the short-tailed fruit bat (*Carollia perspicillata*): comparing theory with measurement. *J. R. Soc. Interface* **11**, 20140147.

Wakeling, J. M. and Ellington, C. P. (1997). Dragonfly flight. II. Velocities, accelerations, and kinematics of flapping flight. *J. Exp. Biol.* **200**, 557-582.

Wang, J. K. and Sun, M. (2005). A computational study of the aerodynamics and forewing-hindwing interaction of a model dragonfly in forward flight. *J. Exp. Biol.* **208**, 3785-3804.

Wang, S., Zhang, X., He, G. and Liu, T. (2013). On applicability of the Kutta-Joukowski theorem to low-Reynolds-number unsteady flows. 51st AIAA Aerospace Sciences Meeting including the New Horizons Forum and Aerospace Exposition, 7-10 January 2013, Grapevine, Texas. *AIAA* 6.2013-6.

Warrick, D. R., Tobalske, B. W. and Powers, D. R. (2009). Lift production in the hovering hummingbird. *Proc. R. Soc. B Biol. Sci.* **276**, 3747-3752.

Weis-Fogh, T. (1973). Quick estimates of flight fitness in hovering animals, including novel mechanisms for lift production. *J. Exp. Biol.* **59**, 169-230.

Willmott, A. P., Ellington, C. P. and Thomas, A. L. R. (1997). Flow visualization and unsteady aerodynamics in the flight of the hawkmoth, *Manduca sexta*. *Philos. Trans. R. Soc. Lond. B Biol. Sci.* **352**, 303-316.

Wootton, R. J. (1981). Support and deformability in insect wings. *J. Zool.* **193**, 447-468.

Young, J., Walker, S. M., Bomphrey, R. J., Taylor, G. K. and Thomas, A. L. R. (2009). Details of insect wing design and deformation enhance aerodynamic function and flight efficiency. *Science* **325**, 1549-1552.

Zhao, L., Huang, Q., Deng, X. and Sane, S. P. (2010). Aerodynamic effects of flexibility in flapping wings. *J. R. Soc. Interface* **7**, 485-497.